IEEE Access
Multidisciplinary | Rapid Review | Open Access Journal

Received September 22, 2018, accepted October 8, 2018, date of publication October 15, 2018, date of current version November 8, 2018.

Digital Object Identifier 10.1109/ACCESS.2018.2875904

Control Design for an Articulated Truck With Autonomous Driving in an Electrified Highway

JESUS FELEZ[1], (Senior Member, IEEE), CARLOS GARCÍA-SANCHEZ[1], AND JOSÉ ANTONIO LOZANO[2]

[1]Mechanical Engineering Department, Universidad Politécnica de Madrid, 28006 Madrid, Spain
[2]Mechanical Engineering, Chemistry and Industrial Design Department, Universidad Politécnica de Madrid, 28012 Madrid, Spain

Corresponding author: Jesus Felez (jesus.felez@upm.es)

ABSTRACT The basis of an electrified highway or eHighway is an intelligent current collector combined with a hybrid drive system, where the eHighway trucks collect power from the overhead cables. The first prototype for these vehicles has been developed by Siemens, but these vehicles need drivers. This paper presents a conceptual model that is an evolution of this approach, proposing a fully electrical vehicle with autonomous driving. This idea has been analyzed through simulations by using a model composed by an articulated truck and its electrical powertrain system, including a control system as well, based the on the model predictive control (MPC), widely used in autonomous vehicles. The vehicle model consists of a 2D model with 10 degrees of freedom, corresponding to the longitudinal and lateral displacements of the tractor, the tractor yaw angle, the semi-trailer yaw angle, and the rotations of the six equivalent wheels. Besides, an electric powertrain system, batteries, and a regenerative brake have been integrated into the model. Several simulation cases have been developed corresponding to an adaptive cruise control, a trajectory tracking, and an overtaking maneuver. The aim of these simulations is also to obtain the minimum size of the battery and its autonomy for an overtaking maneuver, since it is necessary to disconnect the truck from the overhead contact line during this maneuver. The simulations show the viability of this conceptual proposal, obtaining results similar to those expected.

INDEX TERMS Autonomous vehicle, articulated truck, eHighway, electrified highway, model predictive control.

I. INTRODUCTION

In this paper we present the design of a control system for an autonomous driving semi-trailer truck based on Model Predictive Control (MPC). The system is composed by an electric truck powered by an overhead line, being supported by batteries for the cases in which it is necessary to disconnect the pantograph, like in overtaking maneuvers.

Nowadays the road freight transportation dominates the freight transportation sector being significantly higher than the second method of transport (the maritime transport). For this reason, it's necessary to develop new technologies such as *eHighway* proposed by Siemens [1] to reduce the pollution generated by this sector and to be able to satisfy the more demanding legislation. The idea of using an electrical truck connected to an overhead line is part of the Siemen's project, developing an overhead line system in highways to supply with electrical energy the trucks and buses provided with an integrated pantograph as shown in Figure 1.

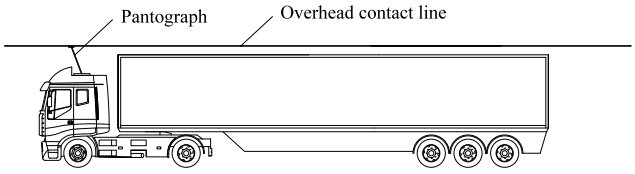

FIGURE 1. eHighway concept.

Sweden and United States are currently implementing this type of highways for testing purposes. In Sweden, Scania in collaboration with Siemens is participating in the design of a hybrid system for the model Scania G 360 4×2 that allows the use of the overhead line. In California Volvo has performed

FIGURE 2. eHighway test in Sweden (picture courtesy of Scania).

some tests with the objective of connecting the harbors of Los Angeles and Long Beach [2]. The purpose of this test is to determine which energy source is the more appropriate to complement the overhead line.

With respect to the electric vehicles, the increasing pressure of the international administrations to reduce the emissions is moving the electric cars into a more advantageous position with respect to their competitors. For example, the regulation Euro VI is intended to reduce dramatically the NOx and PM emissions, which forces the vehicles with diesel engines to implement adsorption equipment that increases the price. In future years the Euro VII is expected to be approved, which is going to be really restrictive with the local contaminants. Therefore, the four types of electric vehicle: BEV (Battery Electric Vehicle), HEV (Hybrid Electric Vehicle), PHV (Plug-in Hybrid Vehicle) and FCEV (Fuel Cell Electric Vehicle), are a serious alternative to occupy the diesel market.

The main challenges of electrical vehicles are their autonomy and their production costs, to position themselves as a more feasible alternative to the diesel vehicles. In the case of the BEV, the improvement in the batteries is crucial. The other problem is how to develop the infrastructure of the battery charging stations.

Another research challenge in the automotive industry are autonomous vehicles, that are defined as the vehicles that are able to recognize its surroundings and imitate the human ability of driving and control [3]. The autonomous capacity that a vehicle has can be measured in 6 levels. Nowadays, different companies are working in the development of level 4 and 5 vehicles [4], even though the highest level that can be found in the market is only level 2 as the Tesla Autopilot or the Nissan ProPilot.

With respect to the control system, the MPC is an advanced control method [5]. It was used for the first time in the beginning of the 70s by Shell Oil. This technique has been successfully used in many industrial applications, like thermal energy control [6], collision avoidance [7], vehicle stability [8], and energy management [9]. The MPC capacity of working with non-linear systems makes it appropriate for several applications in engineering, being of particular interest its use in autonomous vehicles [10].

In the MPC, the model is used to predict the changes in the states of the system produced by the input variables. The system uses the plant measures, the current dynamic states, the limits imposed by the user in the variables and the objective variables to calculate the future changes in the state variables. Thanks to these changes, the state variables can be close to the objective value while satisfying the imposed conditions.

Some companies in the automotive industry like Ford, BMW, Honda, PSA or Toyota are already studying the implementation of this kind of control systems. Its application covers the driving control, the semi active suspension control, the stability control or the energy management in electric vehicles. Even though this type of control system requires a high computational cost, the combination of multi parametric programming and an appropriate design of the prediction horizons can reduce to a suitable time the computational effort for the vehicle microcontrollers, obtaining real time in the real on-board systems. MPC theory and applications to autonomous vehicles can be seen in [11], [12], [13], and [14]. The platooning of autonomous vehicles has also received considerable attention in recent years, due to its potential to significantly benefit road transportation, including improving traffic efficiency, enhancing road safety, and reducing fuel consumption [15], [16], [17], [18], [19]. This idea is applicable for the eHighway concept, but it will be object of future research.

The main contribution of this paper is the development of a model for a trailer with electrical powertrain, as well as the design of its control system for autonomous driving. The model includes the mechanical behavior as well as the electrical behavior for the powertrain. This integrated model is a state-of-the-art contribution for this kind of vehicles.

The remainder of this paper is organized as follows. Section II describes the model for the trailer, powertrain, braking systems and battery. Section describes III the control model. This controller is based in MPC, which is appropriate for this task due to its considerable advantages and its capability to control multivariable systems time-varying being a robust method. Section IV presents the results of several simulations, and Section V includes the conclusions.

II. DYNAMIC MODELS

A. VEHICLE MODEL

The vehicle is composed by two bodies, tractor and semi-trailer, connected with an ideal revolute joint in the kingpin. The vehicle has two axles in the tractor and three axles in the semi-trailer and has been simplified by grouping the three semi-trailer axles in only one equivalent. Each axle has its equivalent left and right wheels. The truck has the driving

system in the tractor rear axle, meanwhile the steering is applied in the front wheels.

With these assumptions, the vehicle model consists of a 2D model with 10 degrees of freedom, corresponding to the x and y displacements of the tractor, the tractor yaw angle, the semi-trailer yaw angle and the rotations of the six equivalent wheels. Figure 3 shows the vehicle schematics and the parameters considered in the model. The values of the parameters used in the model are relegated to Appendix A.

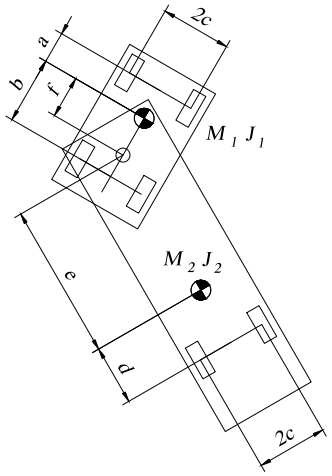

FIGURE 3. Model vehicle schematics and parameters.

A global inertial reference frame $\left[X \; Y \right]$ and two local reference frames $\left[x_1 \; y_1 \right]$ and $\left[x_2 \; y_2 \right]$ are defined.

The tractor is represented as the body 1 and uses subscript 1 and the semitrailer is represented with subscript 2.

Capital letters represent variables referred to the global reference frame, small letters represent variables referred to the local reference frame, and Greek letters represent rotational variables. Figure 4 shows the vehicle variables following the previous notation. The notation is defined as follows:

$\left[X_i \; Y_i \right]$ with $i = 1, 2$ are the c.o.g. (center of gravity) positions referred to the inertial reference frame $\left[X \; Y \right]$ for each body.

$\left[U_i \; V_i \right]$ with $i = 1, 2$ are the c.o.g. velocities referred to the inertial reference frame.

$\left[u_i \; v_i \right]$ with $i = 1, 2$ are the c.o.g. velocities referred to the local reference frame.

φ_i with $i = 1, 2$ are the orientation of the local reference frame with respect to the inertial reference frame.

$s\varphi_i$ means $sin\varphi_i$

$c\varphi_i$ means $cos\varphi_i$

$s\varphi_{ij}$ means $sin(\varphi_i - \varphi_j)$

$c\varphi_{ij}$ means $cos(\varphi_i - \varphi_j)$

ω_i with $i = 1, 2$ are the tractor and semitrailer yaw velocities.

ω_{ij} means $\omega_i - \omega_j$

$X = \left[X_1 \; X_1 \; \varphi_1 \; X_2 \; Y_2 \; \varphi_2 \right]^T$ is the vector of coordinates that represent the system movement in the inertial frame.

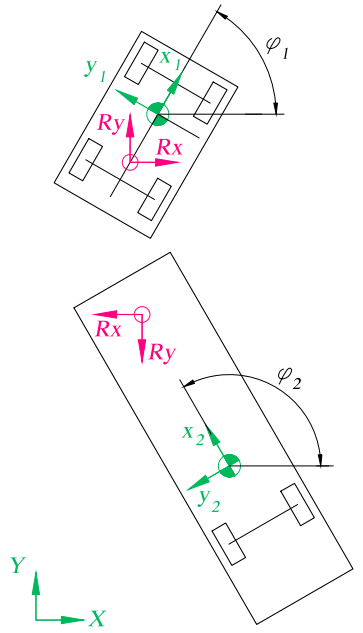

FIGURE 4. Model variables.

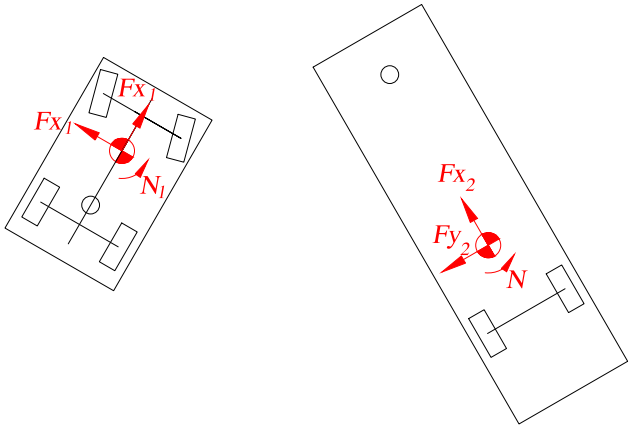

FIGURE 5. Forces and momentums at c.o.g.

$V = \left[U_1 \; V_1 \; \omega_1 \; U_2 \; V_2 \; \omega_2 \right]^T$ is the vector of the c.o.g. velocities referred to the inertial frame.

$v = \left[u_1 \; v_1 \; \omega_1 \; u_2 \; v_2 \; \omega_2 \right]^T$ is the vector of the c.o.g. velocities referred to the local frames.

The forces vector $R = \left[R_x \; R_y \right]^T$ represents the constraint forces at the revolute joint, written in the global reference frame.

Figure 5 includes the different forces considered in the model. In this figure:

$\left[Fx_i \; Fy_i \; N_i \right]$ with $i = 1, 2$ (tractor, semitrailer) are the resultant forces and momentum at c.o.g.

$F_e = \left[Fx_1 \; Fy_1 \; N_1 \; Fx_2 \; Fy_2 \; N_2 \right]^T$ is the vector of the tractor and semitrailer resultant forces and momentums.

The system equations are obtained by applying the Newton' Laws for a multibody system with kinematic constraints. These equations are obtained in the local reference

frame for both bodies and are arranged in a matrix formulation as follows:

$$M \cdot (\dot{v} + v \times \omega) + A \cdot R = F_e \tag{1}$$

The equations (1) are set of six differential equations where the variables are:

$$v = \begin{bmatrix} u_1 & v_1 & \omega_1 & u_2 & v_2 & \omega_2 \end{bmatrix}^T \tag{2}$$

The matrix M is defined as follows:

$$M = \begin{bmatrix} M_1 & 0 & 0 & 0 & 0 & 0 \\ 0 & M_1 & 0 & 0 & 0 & 0 \\ 0 & 0 & J_1 & 0 & 0 & 0 \\ 0 & 0 & 0 & M_2 & 0 & 0 \\ 0 & 0 & 0 & 0 & M_2 & 0 \\ 0 & 0 & 0 & 0 & 0 & J_2 \end{bmatrix} \tag{3}$$

and, because v is in local frames,

$$\dot{v} + v \times \omega = \begin{bmatrix} \dot{u}_1 - v_1\omega_1 \\ \dot{v}_1 + u_1\omega_1 \\ \dot{\omega}_1 \\ \dot{u}_2 - v_2\omega_2 \\ \dot{v}_2 + u_2\omega_2 \\ \dot{\omega}_2 \end{bmatrix} \tag{4}$$

System equations (1) include also the vector R with two additional variables that represent the two constraint forces at the revolute joint.

The expressions of the constraint equations, written in terms of velocities in the inertial frame are:

$$\Phi = \begin{bmatrix} U_1 + f\omega_1 s\varphi_1 - U_2 + e\omega_2 s\varphi_2 \\ V_1 - f\omega_1 c\varphi_1 - V_2 - e\omega_2 c\varphi_2 \end{bmatrix} = \begin{bmatrix} 0 \\ 0 \end{bmatrix} \tag{5}$$

The matrix A in (1) has the following expression:

$$A = T \cdot J^T \tag{6}$$

where

$$T = \begin{bmatrix} c\varphi_1 & s\varphi_1 & 0 & 0 & 0 & 0 \\ -s\varphi_1 & c\varphi_1 & 0 & 0 & 0 & 0 \\ 0 & 0 & 1 & 0 & 0 & 0 \\ 0 & 0 & 0 & c\varphi_2 & s\varphi_2 & 0 \\ 0 & 0 & 0 & -s\varphi_2 & c\varphi_2 & 0 \\ 0 & 0 & 0 & 0 & 0 & 1 \end{bmatrix} \tag{7}$$

and J is the Jacobian matrix obtained from the constraint equations at the revolute joint. The Jacobian matrix J is obtained as follows:

$$J = {}^{\partial\Phi}/_{\partial V} \tag{8}$$

Then, the transposed Jacobian matrix J^T is written as:

$$J^T = \begin{bmatrix} 1 & 0 \\ 0 & 1 \\ fs\varphi_1 & -f\,c\varphi_1 \\ -1 & 0 \\ 0 & -1 \\ es\varphi_2 & -e\,c\varphi_2 \end{bmatrix} \tag{9}$$

Thus, the expression of A results as:

$$A = \begin{bmatrix} c\varphi_1 & s\varphi_1 \\ -s\varphi_1 & c\varphi_1 \\ f\,s\varphi_1 + e\,s\varphi_2 & -fc\varphi_1 - e\,c\varphi_2 \\ -c\varphi_2 & -s\varphi_2 \\ s\varphi_2 & -c\varphi_2 \\ e\,s\varphi_2 & -e\,c\varphi_2 \end{bmatrix} \tag{10}$$

Moreover, to know the position in global coordinates, it is necessary to add the following equations:

$$\begin{bmatrix} \dot{X}_1 \\ \dot{Y}_1 \\ \dot{\varphi}_1 \\ \dot{X}_2 \\ \dot{Y}_2 \\ \dot{\varphi}_2 \end{bmatrix} = \begin{bmatrix} c\varphi_1 & -s\varphi_1 & 0 & 0 & 0 & 0 \\ s\varphi_1 & c\varphi_1 & 0 & 0 & 0 & 0 \\ 0 & 0 & 1 & 0 & 0 & 0 \\ 0 & 0 & 0 & c\varphi_2 & -s\varphi_2 & 0 \\ 0 & 0 & 0 & s\varphi_2 & c\varphi_2 & 0 \\ 0 & 0 & 0 & 0 & 0 & 1 \end{bmatrix} \begin{bmatrix} u_1 \\ v_1 \\ \omega_1 \\ u_2 \\ v_2 \\ \omega_2 \end{bmatrix} \tag{11}$$

Then, the vehicle dynamics equations are a set of $6 + 2 + 6$ equations obtained from (1), (5) and (11), formed by a subset of 12 differential equations (1) and (11) and a subset of two algebraic equations (5).

These differential-algebraic equations can be optimized and reduced to a set of differential equations by eliminating the algebraic constraints. Then, following the proposed procedure in [20] and [21], two dependent velocities are eliminated, and the equations (1) will be expressed only in terms of four independent velocities. In this case the dependent velocities chosen are the semi-trailer velocities (u_2 v_2).

In order to do so, it is necessary to define a matrix S, that projects all the velocities into the independent ones. This matrix is written as:

$$S = \begin{bmatrix} 1 & 0 & 0 & 0 \\ 0 & 1 & 0 & 0 \\ 0 & 0 & 1 & 0 \\ c\varphi_{12} & -s\varphi_{12} & f\,s\varphi_{12} & 0 \\ s\varphi_{12} & c\varphi_{12} & -f\,c\varphi_{12} & -e \\ 0 & 0 & 0 & 1 \end{bmatrix} \tag{12}$$

Then:

$$\begin{bmatrix} u_1 \\ v_1 \\ \omega_1 \\ u_2 \\ v_2 \\ \omega_2 \end{bmatrix} = S \begin{bmatrix} u_1 \\ v_1 \\ \omega_1 \\ \omega_2 \end{bmatrix} \tag{13}$$

and

$$\begin{bmatrix} \dot{u}_1 \\ \dot{v}_1 \\ \dot{\omega}_1 \\ \dot{u}_2 \\ \dot{v}_2 \\ \dot{\omega}_2 \end{bmatrix} = \dot{S} \begin{bmatrix} u_1 \\ v_1 \\ \omega_1 \\ \omega_2 \end{bmatrix} + S \begin{bmatrix} \dot{u}_1 \\ \dot{v}_2 \\ \dot{\omega}_1 \\ \dot{\omega}_2 \end{bmatrix} \tag{14}$$

Finally, substituting (14) in (1) and pre-multiplying by S^T we obtain:

$$\begin{bmatrix} M_1+M_2 & 0 & 0 & -M_2 e s\varphi_{12} \\ 0 & M_1+M_2 & -M_2 f & -M_2 e\, c\varphi_{12} \\ 0 & -M_2 f & J_1+M_2 f^2 & M_2 e f\, c\varphi_{12} \\ -M_2 e\, s\varphi_{12} & -M_2 e\, c\varphi_{12} & M_2 e f\, c\varphi_{12} & J_2+M_2 e^2 \end{bmatrix} \begin{bmatrix} \dot{u}_1 \\ \dot{v}_2 \\ \dot{\omega}_1 \\ \dot{\omega}_2 \end{bmatrix}$$
$$= \begin{bmatrix} 0 & M_2\omega_{12} & -M_2 f\,\omega_{12} & 0 \\ -M_2\omega_{12} & 0 & 0 & 0 \\ M_2 f\,\omega_{12} & 0 & 0 & 0 \\ M_2 e\omega_{12} c\varphi_{12} & -M_2 e\omega_{12} s\varphi_{12} & M_2 e f\,\omega_{12} s\varphi_{12} & 0 \end{bmatrix} \begin{bmatrix} u_1 \\ v_1 \\ \omega_1 \\ \omega_2 \end{bmatrix}$$
$$+ \begin{bmatrix} M_1\omega_1 v_1 + M_2\omega_2\,(v_1 - f\omega_1 - e\omega_2\, c\varphi_{12}) \\ -M_1\omega_1 u_1 - M_2\omega_2\,(u_1 - e\omega_2\, s\varphi_{12}) \\ M_2 f\,\omega_2\,(u_1 - e\omega_2\, s\varphi_{12}) \\ M_2 e\omega_2\,(u_1 c\varphi_{12} - (v_1 - f\omega_1)\, s\varphi_{12}) \end{bmatrix}$$
$$+ \begin{bmatrix} Fx_1 + Fx_2\, c\varphi_{12} + Fy_2\, s\varphi_{12} \\ Fy_1 - Fx_2\, s\varphi_{12} + Fy_2\, c\varphi_{12} \\ N_1 + Fx_2 f\, s\varphi_{12} - Fy_2 f\, c\varphi_{12} \\ -eFy_2 + N_2 \end{bmatrix} \tag{15}$$

And (11) remains as:

$$\begin{bmatrix} \dot{X}_1 \\ \dot{Y}_1 \\ \dot{\varphi}_1 \\ \dot{\varphi}_2 \end{bmatrix} = \begin{bmatrix} c\varphi_1 & -s\varphi_1 & 0 & 0 \\ s\varphi_1 & c\varphi_1 & 0 & 0 \\ 0 & 0 & 1 & 0 \\ 0 & 0 & 0 & 1 \end{bmatrix} \begin{bmatrix} u_1 \\ v_1 \\ \omega_1 \\ \omega_2 \end{bmatrix} \tag{16}$$

B. MODEL FORCES

The forces F_e are obtained from the external forces and the tire forces with the following expressions:

$$Fx_1 = Tx_{fr} + Tx_{fl} + Tx_{rr} + Tx_{rl} - \delta(Ty_{fr} + Ty_{fl}) - F_a \tag{17}$$
$$Fy_1 = Ty_{fr} + Ty_{fl} + Ty_{rr} + Ty_{rl} + \delta(Tx_{fr} + Tx_{fl}) \tag{18}$$
$$N_1 = a\left(Ty_{fr} + Ty_{fl}\right) - b\left(Ty_{rr} + Ty_{rl}\right) + c(Tx_{fr} + Tx_{rr} - Tx_{fl} - Tx_{rl}) \tag{19}$$
$$Fx_2 = Tx_{sr} + Tx_{sl} \tag{20}$$
$$Fy_2 = Ty_{sr} + Ty_{sl} \tag{21}$$
$$N_2 = -d\left(Ty_{sr} + Ty_{sl}\right) + c\left(Tx_{sr} - Tx_{sl}\right) \tag{22}$$

Figure 6 shows these forces, where the angle δ denotes the steering angle. In this figure:

$\left[\, Tx_{ij}\ Ty_{ij} \,\right]$ with $i = f, r$ (front, rear) and $j = l, r$ (left, right) are the tractor tire forces.

$\left[\, Tx_{ij}\ Ty_{ij} \,\right]$ with $i = s$ (semitrailer) and $j = l, r$ (left, right) are the semitrailer tire forces.

F_a is a sum of the longitudinal external forces including the aerodynamic drag, the rolling resistance and the slope resistance.

The lateral tire forces Ty_{ij} are obtained from the slip angle α_{ij}, that depends on the relation between the lateral and longitudinal wheel speed on the ground contact point, according to the following expressions:

$$\alpha_{fj} = {}^{v_{fj}}\!/_{u_{fj}} - \delta \quad j = l, r \tag{23}$$
$$\alpha_{ij} = {}^{v_{ij}}\!/_{u_{ij}} \quad i = r, s j = l, r \tag{24}$$

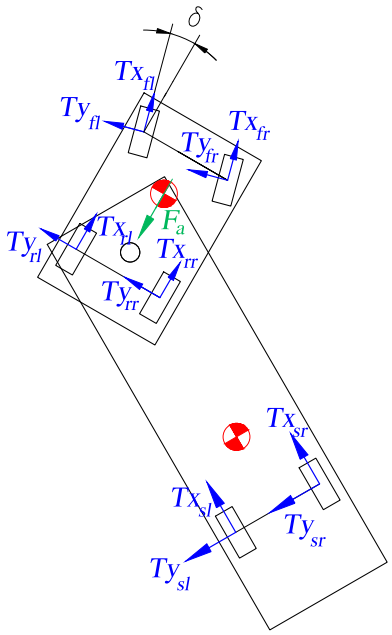

FIGURE 6. Tire forces and aerodynamic drag.

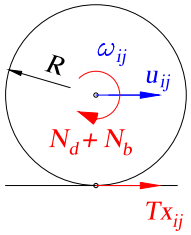

FIGURE 7. Wheel rotation dynamics.

The model assumes small steering angles so $\sin\delta \cong \delta$ and $\cos\delta \cong 1$. Expression (23) allows to determine the slip angle of the front tractor wheels, including the steering angle, and (24) represents the slip angle for the tractor rear wheels α_{rj} and for the semitrailer wheels α_{sj}.

Then, considering linear behavior for the tires, Ty_{ij} is obtained by multiplying the slip angle by the cornering stiffness Cy_{ij} (25).

$$Ty_{ij} = -Cy_{ij}\,\alpha_{ij} \tag{25}$$

The tire longitudinal forces are obtained from the wheel rotation dynamics by using the slip ratio s. Following [22] the equation governing the wheel rotation is:

$$I_{\mathrm{ij}}\dot{\omega}_{\mathrm{ij}} = N_d - N_{rb} - N_{pb} - RTx_{ij} \tag{26}$$

where, for the wheel ij, Tx_{ij} is the longitudinal tire force, ω_{ij} is the angular velocity, N_d is the driving torque, N_{rb} is the regenerative braking torque,N_{pb} is the pneumatic braking torque, I_{ij} is the wheel inertia, and R is the wheel dynamic radius under load.

Figure 7 shows the wheel rotation movement and its involved variables.

The forces Tx_{ij} are calculated by using the slip ratio s defined as (27) when driving and (28) when braking:

$$s_{ij} = 1 - {R\omega_{ij}}/{u_{ij}} \tag{27}$$

$$s_{ij} = 1 - {u_{ij}}/{R\,\omega_{ij}} \tag{28}$$

Then,

$$Tx_{ij} = Cx_{ij}\, s_{ij} \tag{29}$$

C. ELECTRICAL DRIVING SYSTEM. ELECTRIC MOTOR AND BATTERIES

Moreover, the vehicle model needs several additional characteristics such as the introduction of a model for electrical driving, being capable to connect and disconnect from the overhead power line through a pantograph, a regenerative braking system to recover part of the energy lost when braking, and a model for the batteries in case of driving disconnected from the overhead line. We assume the same driving/braking torque in both wheels in the same axle.

1) ELECTRICAL DRIVING MODEL

For the driving model, we have considered a simple model in which the driving power is bounded by the maximum effective driving power P_d.

$$2u_1 RN_d \leq P_d \tag{30}$$

where:

u_1 is the tractor longitudinal velocity

N_d is the driving force

P_d is the maximum effective driving power

R is the wheel radius

This driving force is limited by the wheel adherence.

$$RN_d \leq F_{max} \tag{31}$$

where:

F_{max} is the maximum force at the ground, limited by the adherence.

To model the connection with the electrical network, the power line is assumed as a constant source of 700 V, therefore the intensity is calculated as the necessary to give the motor the required power.

The motor behavior is governed by the equations (32):

$$\begin{aligned} L_M \frac{di_M}{dt} &= V_0 - T_M \omega_M - R_M\, i_M \\ N_d &= T_M\, i_M \end{aligned} \tag{32}$$

where:

ω_M is the angular velocity in the rotor, obtained as $(\omega_l + \omega_r)/2$

i_M is the current intensity in the motor

L_M is the inductance

R_M is the internal resistance

V_0 is the voltage source, obtained from the overhead line or from the battery

T_M is the slope of the motor curve $V = f(\omega)$ linearized at the operating point.

2) BRAKING SYSTEM

The vehicle braking system uses two mechanisms: a pneumatic braking and a regenerative braking system. The pneumatic brake is applied on all the wheels, meanwhile the regenerative brake is applied only on the driving wheels.

The regenerative braking system is modeled in the same way that the traction system, obtaining the following equations (33)

$$\begin{aligned} u_1 RN_{rb} &\leq P_{rb} \\ RN_{rb} &\leq F_{max} \end{aligned} \tag{33}$$

The pneumatic braking system is modeled in a similar way as the regenerative braking (34)

$$\begin{aligned} 2 \cdot (c_1 u_1 + c_2 u_2)\, RN_{pb} &\leq P_{pb} \\ RN_{pb} &\leq F_{max} \end{aligned} \tag{34}$$

where:

u_1 is the tractor longitudinal velocity

u_2 is the semitrailer longitudinal velocity, with $u_2 = c\varphi_{12} u_1 - s\varphi_{12} v_1 + f s\varphi_{12} \omega_1$

N_{rb} is the regenerative braking torque

P_{rb} is the maximum effective regenerative braking power

N_{pb} is the pneumatic braking torque

P_{pb} is the maximum effective pneumatic braking power

c_1 and c_2 are the pneumatic braking distribution coefficients between tractor and semitrailer.

3) BATTERIES

The battery follows the model presented in [23] and [24]. The circuit in Figure 8 represents the SOC estimation model. Assuming that a battery is discharged from an equally charged state to the same end-of-discharge voltage, the extracted energy, called usable capacity, is modeled by a full-capacity capacitor C_C and a self-discharge resistor R_S.

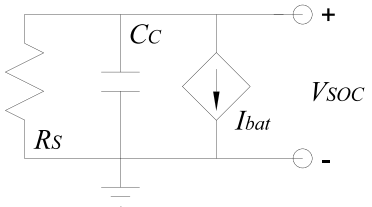

FIGURE 8. SOC estimation model.

The full-capacity capacitor C_C represents the whole charge stored in the battery, i.e., the state of charge SOC, and its value is defined as (35):

$$C_C = 3600 \cdot C_0 \cdot f_1 \cdot f_2 \cdot f_3 \tag{35}$$

where C_0 is the nominal capacity in Ah and f_1, f_2, f_3 are correction factors of the charge/discharge rate, temperature and cycle number.

By setting the initial voltage across C_C (V_{SOC}) equal to 1 V or 0 V, the battery is initialized to its fully charged (i.e., SOC is 100%) or fully discharged

(i.e., SOC is 0%) states. In other words, V_{SOC} represents the SOC of the battery quantitatively.

Then, the SOC is obtained from the following equation:

$$SOC = SOC_0 + \int_0^t \zeta \cdot i_{bat}(t)/C_C dt \tag{36}$$

where ζ is a constant to normalize (36) to the battery capacity, SOC ranges between 0 and 100% and i_{bat} is the intensity in the battery.

Figure 9 shows the model proposed for predicting terminal voltage and power losses in the battery and is built upon [23].

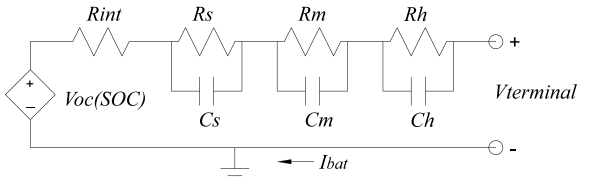

FIGURE 9. Model for terminal voltage and losses.

In this circuit, each parameter is a function of the SOC [1], i.e. $V_{oc}, R_{int}, R_s, R_m, R_h, C_s, C_m, C_h$ depend on the SOC. The polynomial expression (37) takes into consideration those SOC dependences:

$$\begin{aligned}(V_{oc}, R_{series}, R_s, R_m, R_h, C_s, C_m, C_h) \\ = a_0 + a_1 \cdot SOC + a_2 \cdot SOC^2 + a_3 \cdot SOC^3 \\ + a_4 \cdot SOC^4 + a_5 \cdot SOC^5 + a_6 \cdot SOC^6\end{aligned} \tag{37}$$

The values of the different coefficients and parameters of the model are included in Appendix B.

Then:

$$V_{terminal} = V_{oc} - i_{bat} \cdot R_{int} - i_{bat} \cdot R_{trans} \tag{38}$$

where:

$V_{terminal}$ is the output cell voltage

i_{bat} is the current intensity at the battery

R_{trans} is the equivalent resistance obtained from R_{int}, R_s, R_m, R_h, C_s, C_m, C_h

V_{oc} is the open circuit voltage

To calculate the necessary cells in parallel Cel_{par}, we use the vehicle autonomy as the sizing criterion, according to the following formula:

$$Cel_{par} = \frac{P_{max} \cdot t_{aut}}{Cap \cdot Cel_{ser} \cdot V_{terminal}} \tag{39}$$

where

P_{max} is the motor power

t_{aut} is the time autonomy for the battery

Cap is the capacity for each cell

Cel_{ser} is the number of cells in series

D. COUPLING BETWEEN WHEELS AND ELECTRICAL POWER

Figure 10 shows the coupling between the different systems when the battery is connected. The state ω coming from the wheel (26) is used in (32) to obtain the state i_M in the motor and the battery provides the needed voltage coming from (38).

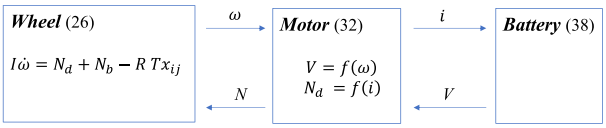

FIGURE 10. Connection to battery.

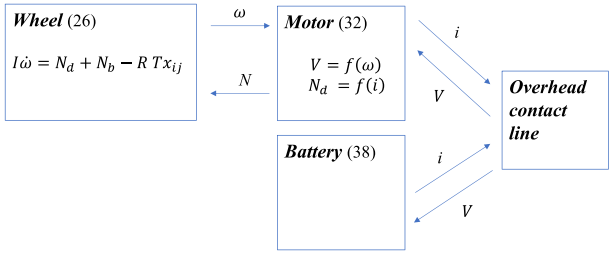

FIGURE 11. Connection to overhead contact line.

Figure 11 describes the coupling when the vehicle is connected to the overhead line, showing how it provides voltage to the motor and for charging the battery.

III. DESIGN OF THE MPC CONTROLLER

A. PROBLEM DESCRIPTION

Regrouping the previous expressions (15), (16), (26), (32), (36) and (38) the system equations for the vehicle dynamics are written in a compacted way as:

$$\dot{x} = f_v(x, U) \tag{40}$$

where:

$x = \left[v_i^T \; X_i^T \; \omega_i^T \; e_i^T \right]^T$ is a vector including the states.

$v_i = \left[u_1 \; v_1 \; \omega_1 \; \omega_2 \right]^T$ is vector with the independent velocities.

$X_i = \left[X_1 \; Y_1 \; \varphi_1 \; \varphi_2 \right]^T$ includes the global positions and orientations for tractor and semitrailer.

$\omega_i = \left[\omega_{fr} \; \omega_{fl} \; \omega_{rr} \; \omega_{rl} \; \omega_{sr} \; \omega_{sl} \right]^T$ includes the wheels angular velocity.

$e_i = \left[i_M \; i_{bat} \; SOC \right]^T$ are the electrical states.

$U = \left[N_d \; N_{rb} \; N_{pb} \; \delta \right]^T$ is a vector including the inputs.

B. OPTIMAL CONTROL DESIGN

A Model Predictive Control (MPC) approach is proposed for the vehicle. MPC is selected due to its capability of systematically handling multiple input and state constraints, which in this problem are critical. According to the receding horizon principle, at each time step the MPC algorithm computes the optimal control and the state trajectories, solving a finite horizon optimization problem.

For the formulation of the MPC a prediction horizon $\left[t, t + N_p\right]$ is considered at time t. The notation $x_{t+k|t}$ represents the state vector at time $t+k$, predicted at time t, obtained by starting from the current state $x_{t|t} = x\,(t) \equiv x_t$, and where $U_{\cdot|t} = \left[U_{t|}t, \ldots, U_{t+N_p-1|t}\right]$ denotes the unknown input variables to be optimized. As previously stated, the subscript 1 denotes the tractor and subscript 2 denotes the semitrailer.

1) SYSTEM DYNAMICS

Equations (41) represent the system dynamics updates for the discrete-time model obtained from (40). The initial state is set in (42).

$$x_{k+1|t} = f\left(x_{k|t}, U_{k|t}\right) \quad \forall k = t, \ldots t + N_p - 1 \tag{41}$$

$$x_{t|t} = x_t \tag{42}$$

2) FRONT VEHICLE

Two different types of vehicles that can interact with the truck are considered.

We denote as preceding vehicle the vehicle that is in the same lane. Both vehicles, the truck and the preceding one are circulating in the same direction. The truck has two possibilities: to follow the preceding at a safe distance, or to overtake it.

We denote as front vehicle the vehicle that is in the left lane. This vehicle must be considered in the overtaking maneuver. The preceding vehicle magnitudes are denoted with superscript p, while the front vehicle magnitudes are denoted with superscript f.

Then u^p is defined as the longitudinal velocity for the preceding vehicle and u^f is the velocity for the front vehicle.

In this study, both velocities are considered as estimated variables for the truck MPC control and are obtained from a simple point mass model that follows a preestablished trajectory and a predefined speed profile.

3) TRAJECTORY TRACKING

For the trajectory tracking, it is necessary to define two reference points P_1 and P_2. These points are represented in Figure 12.

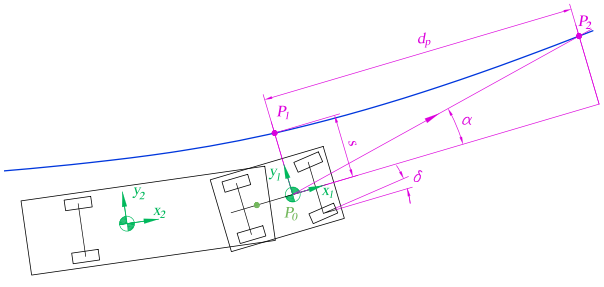

FIGURE 12. Trajectory tracking.

Assuming that the truck direction is approximately parallel to the desired trajectory, P_1 is defined as the point in the lateral direction of the tractor (y_1) belonging to the desired trajectory. Then s is the distance between P_0 and P_1.

P_2 is defined as a point in the desired trajectory that is ahead at a distance d_p. Then α is calculated as the angle between the line $P_0 - P_2$ and the truck local axis x_1

The distance s and the angle α will be used in the cost function as variables to be minimized.

4) MODEL CONSTRAINTS

a: INPUT CONSTRAINTS

The driving and braking forces must be bounded by:

$$0 \leq RN_{d_{k|t}} \leq F_{max} \tag{43}$$

$$-F_{max} \leq RN_{rb_{k|t}} \leq 0 \tag{44}$$

$$-F_{max} \leq RN_{pb_{k|t}} \leq 0 \tag{45}$$

$$-F_{max} \leq RN_{rb_{k|t}} + RN_{pb_{k|t}} \leq 0 \tag{46}$$

$$0 \leq u_{1_{k|t}} \cdot RN_{d_{k|t}} \leq P_d \tag{47}$$

$$-P_b \leq u_{1_{k|t}} \left(RN_{rb_{k|t}} + c_1 RN_{pb_{k|t}}\right) + u_{2_{k|t}} c_2 RN_{pb_{k|t}} \leq 0 \tag{48}$$

where $P_b = P_{rb} + P_{pb}$.

$$-\delta_{max} \leq \delta_{k|t} \leq \delta_{max} \quad \forall k = t, \ldots, t + N_p - 1 \tag{49}$$

The input constraints include the limitation of the maximum driving and braking force and the power limitation in driving and braking. Equations (43) and (47) represent the maximum driving force and the maximum power for the electric driving and regenerative braking. Constraints (44) and (45) represent the force limitation for both braking systems. Constraint (46) means that when the regenerative and pneumatic brakes are simultaneously acting they have the same force limitation that when only electrical braking system is necessary, and equation (48) stablishes the power limitation when both systems act at the same time. Constraint (49) bounds the steering angle.

In the MPC formulation, we will refer to these constraints as $u_{k|t} \in \mathbb{U}_{k|t}$.

b: SPEED CONSTRAINT

In order to guarantee that the vehicle respects the speed limit, the speed is bounded by the following constraint:

$$v_{min} \leq u_{1_{k|t}} \leq v_{max} \quad \forall k = t, \ldots, t + N_p - 1 \tag{50}$$

In the MPC, we will refer to this constraint as $v_{k|t} \in \mathbb{V}_{k|t}$.

c: DYNAMICS CONSTRAINTS

In order to guarantee the pitch and yaw stability, the lateral and yaw speeds are bounded by the following constraints:

$$-a_{max}\Delta t \leq v_{1_{k+1|t}} - v_{1_{k|t}} \leq a_{max}\Delta t \tag{51}$$

$$-\gamma_{max}\Delta t \leq \omega_{1_{k+1|t}} - \omega_{1_{k|t}} \leq a\gamma_{max}\Delta t \tag{52}$$

$$-\gamma_{max}\Delta t \leq \omega_{12_{k+1|t}} - \omega_{12_{k|t}} \leq a\gamma_{max}\Delta t \quad \forall k = t, \ldots, t + N_p - 1 \tag{53}$$

Constraint (51) stablishes a limitation of the lateral acceleration, used to prevent the trailer overturn. Constraint (52) limits the yaw acceleration obtaining softer steering maneuvers. And constraint (53) prevents the well-known yaw instability in trailers [25]. Δt denotes the sample time.

In the MPC formulation, we will refer to these constraints as $x_{k|t} \in \mathbb{X}_{k|t}$.

d: SOC CONSTRAINT

The SOC is bounded by the following constraint (54):

$$0.5 \leq SOC_{k|t} \leq 1 \quad \forall k = t, \ldots, t + N_p - 1 \tag{54}$$

The reason is that the vehicle must preserve a safe *SOC* when it's overtaking and is disconnected of the overhead line.

In the MPC formulation, we will refer to this constraint as $SOC_{k|t} \in \mathbb{S}_{k|t}$.

e: SAFETY CONSTRAINT

It is necessary to introduce a constraint that guarantees that the truck state lies always in a safety region. This is done in the MPC formulation by guaranteeing that in the worst case of a preceding vehicle full-braking, or in the worst case of a front vehicle fully accelerating when overtaking, the truck is able to stop behind the preceding one.

This is done with terminal constraints. They are imposed to guarantee that the controller is recursively feasible and safe.

In the following maneuver, it guarantees that the truck can come to a full stop without collision when the preceding vehicle performs an emergency braking with the maximum deceleration a^p and the truck brakes with $a^t < a^p$ (55).

$$d^p_{t+N_p|t} + \frac{\left(u_{p_{t+N_p|t}}\right)^2}{2a^p} - \frac{\left(u_{1_{t+N_p|t}}\right)^2}{2a^t} - d_{min} \geq 0 \tag{55}$$

being d_{min} the safety distance and $d^p_{t+N_p|t}$ the distance between the truck and the preceding vehicle calculated as:

$$d^p_{t+N_p|t} = \sqrt{\left(X^p_{t+N_p|t} - X_{1\,t+N_p|t}\right)^2 + \left(Y^p_{t+N_p|t} - Y_{1\,t+N_p|t}\right)^2} \tag{56}$$

In the MPC formulation, we will refer to this constraint as $d^p_{safe_{t+N_p|t}} \geq 0$

In the overtaking maneuver, it guarantees that the truck can come to a full stop without collision when the front vehicle is approximating with the maximum acceleration a^f (57).

$$d^f_{t+N_p|t} + \frac{\left(u_{f_{t+N_p|t}}\right)^2}{2a^f} + \frac{\left(u_{1_{t+N_p|t}}\right)^2}{2a^t} - d_{min} \geq 0 \tag{57}$$

being $d^f_{t+N_p|t}$ the distance between the truck and the front vehicle calculated as:

$$d^f_{t+N_p|t} = \sqrt{\left(X^f_{t+N_p|t} - X_{1\,t+N_p|t}\right)^2 + \left(Y^f_{t+N_p|t} - Y_{1\,t+N_p|t}\right)^2} \tag{58}$$

If the vehicle in the left lane is circulating in the same direction, such as in a highway, the constraint will be as (55).

In the MPC formulation, we will refer to this constraint as $d^f_{safe_{t+N_p|t}} \geq 0$.

Both constraints (55) and (57) are incompatible between them, i.e., when the truck is in its lane, constraint (57) is deactivated and (55) is active. On the other hand, when the truck is overtaking, constraint (55) is deactivated and (57) is active.

5) COST FUNCTION

The objective of the truck is to circulate at the maximum speed, i.e. following the preceding vehicle at a safe distance and overtaking when the maneuver is safe. The way to perform this is to activate or deactivate constraints (55) and (57) checking the distance with the preceding car and with the front car.

Therefore, the objective function is defined as follows:

$$J(x, U) = \sum_{k=t}^{t+N_p} K_V \left(u_{1_{k|t}} - u_{des}\right)^2 \tag{59}$$

$$+ \sum_{k=t}^{t+N_p} K_U \left(U_{pb_{k|t}}\right)^2 \tag{60}$$

$$+ \sum_{k=t}^{t+N_p} K_s \left(s_{k|t}\right)^2 \tag{61}$$

$$+ \sum_{k=t}^{t+N_p} K_\alpha \left(\alpha_{k|t}\right)^2 \tag{62}$$

The different terms in the cost function (59) to (62) have the following meaning: $K_V \geq 0$ represents the weight penalizing the output deviation from the truck maximum desired speed, being u_{des} the maximum desired speed. $K_U \geq 0$ represents the weight penalizing the pneumatic braking, prioritizing the regenerative brake. $K_s \geq 0$ represents the weight penalizing the lateral displacement in the trajectory tracking. $K_\alpha \geq 0$ represents the weight penalizing the orientation error in the trajectory tracking.

6) MODEL PREDICTIVE CONTROL FORMULATION

The objective of the control system is to follow the preceding vehicle at a safe distance overtaking it when possible, while satisfying the state and input constraints. Therefore, the optimization problem is formulated as:

$$\min_{U_{.|t}} J(x, U) \tag{63}$$

subject to:

$$x_{k+1|t} = f(x_{k|t}, U_{k|t}) \tag{64}$$

$$U_{k|t} \in \mathbb{U}_{k|t} \tag{65}$$

$$v_{k|t} \in \mathbb{V}_{k|t} \tag{66}$$

$$SOC_{k|t} \in \mathbb{S}_{k|t} \quad \forall k = t, \ldots, t + N_p - 1 \tag{67}$$

$$x_{t|t} = x_t \tag{68}$$

$$\begin{cases} d^p_{safe_{t+N_p|t}} \geq 0 \\ or \\ d^f_{safe_{t+N_p|t}} \geq 0 \end{cases} \tag{69}$$

The resulting optimal states and inputs of (63)-(69) are denoted as following:

$$x^*_t = \left(x^*_{t|t}\ x^*_{t+1|t}\ \cdots\ x^*_{t+N_p|t}\right)^T$$

$$U^*_t = \left(U^*_{t|t}\ U^*_{t+1|t}\ \cdots\ U^*_{t+N_p|t}\right)^T \tag{70}$$

For closing the loop, the first input is applied to the system (40) during the time interval $[t, t+1)$

$$U_t = U^*_{t|t} \tag{71}$$

At the next time step $t+1$, a new optimal problem in the form of (63)-(69) is solved over a shifted horizon, based on a new states measurement.

IV. SIMULATIONS

Several cases have been developed for the design and validation through simulation, corresponding to the implementation of a conventional cruise control, integration of adaptive cruise control, trajectory tracking control, overtaking control and battery dimensioning.

The control system includes at the same time cruise control and trajectory tracking, established by the terms (59), (61) and (62) of the cost function. So they are always considered. The battery management is considered by the constraint (54), being applied to the model only when the vehicle is disconnected from the contact line, i.e., in the overtaking maneuver. The overtaking maneuver is activated by means of its corresponding constraint depending on the traffic conditions, as will be explained in the subsection *C*.

A. ADAPTIVE CRUISE CONTROL

The adaptive cruise control calculates the necessary speed to maintain a safe distance from the preceding vehicle.

In this case, the vehicle is always connected to the overhead line, so the SOC constraint for the battery is not considered, and overtaking is not considered, because the goal of this simulation is to analyze the adaptive cruise control.

The safety distance d_{min} is obtained by using a common spacing policy as shown in [26], having a constant term d_0 that represents the minimum inter-vehicle distance, and a second term that is linearly dependent on the preceding vehicle speed u_p. The coefficient k_f is the time-headway corresponding to the minimum inter-vehicle distance. Then, the expression used to calculate the safety distance is:

$$d_{min} = d_0 + k_f \cdot u_p \tag{72}$$

The values of the different coefficients are obtained by taking as reference the "*Volvo Enhanced Adaptive Cruise Control*" [27]. For this system, the default following distance is almost 76 m travelling at 95 km/h, so we consider the following values:

$$d_0 = 40, \quad k_f = 1,5 \tag{73}$$

The preceding vehicle speed u_p is estimated based on the distance between both vehicles, according to the following expression:

$$u_p = u_1 + {}^{d_p}/_{\Delta t} \tag{74}$$

The distance is calculated as:

$$d_p = \sqrt{\left(X^p_{t+1} - X_{1t}\right)^2 + \left(Y^p_{t+1} - Y_{1t}\right)^2} \tag{75}$$

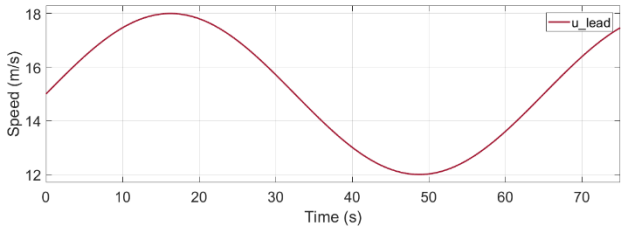

FIGURE 13. Leader speed.

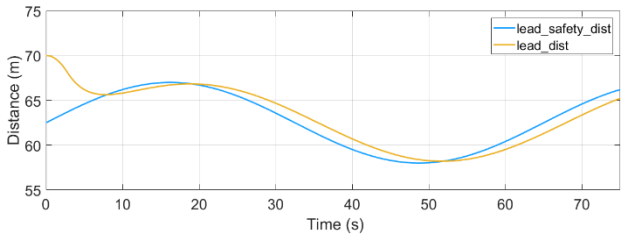

FIGURE 14. Distance between both vehicles.

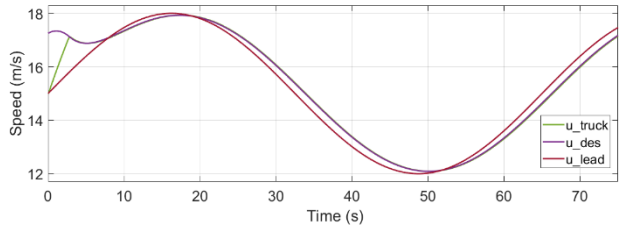

FIGURE 15. Speeds for both vehicles.

Then the vehicle calculates its desired speed u_{des} as:

$$u_{des} = u_p + k \cdot (d_p - d_{min}) \tag{76}$$

1) LEADER AT VARIABLE SPEED

For this simulation we define an initial speed of 15 m/s and an initial distance between both vehicles of 70 m. The speed for the preceding vehicle or leader is variable and is shown in Figure 13.

Figure 14 shows the distance between the two vehicles and the safety distance calculated by the truck depending on the leader speed.

As seen in Figure 14, at the beginning, both vehicles are separated by a greater distance (yellow) than the safety distance (blue) calculated. Therefore, the truck accelerates towards the leader. Once reached, the truck adjusts its speed maintaining a safe distance.

Figure 15 shows the speeds during the simulation. The truck speed is displayed in green, the desired calculated speed in purple and the leader speed in magenta. At the beginning, the truck speed must be higher than the leader one, since the distance is greater than the desired one. Then, the trailer approximates its speed to the one of the vehicle ahead and it's also trying to reach the safety distance.

Figure 16 shows the normalized driving force (driving force divided by maximum force allowed). At the beginning, it accelerates to the maximum to reach the safety distance.

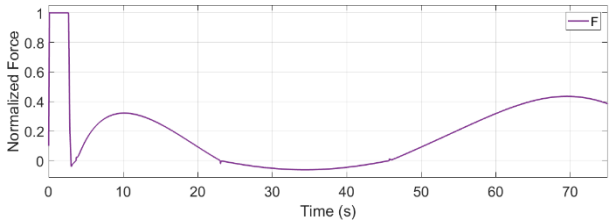

FIGURE 16. Accelerator / brake force during adaptive cruise control simulation.

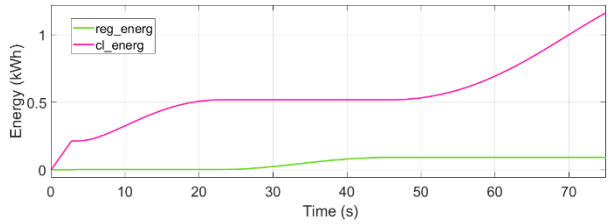

FIGURE 17. Consumed and regenerated energy during the adaptive cruise control simulation.

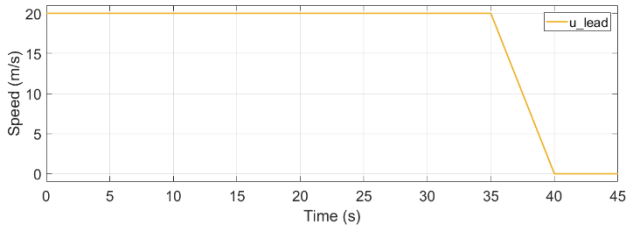

FIGURE 18. Leader velocity.

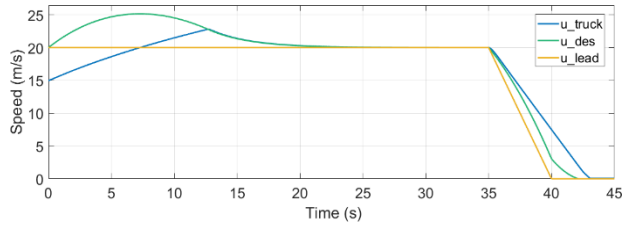

FIGURE 19. Speeds during the braking maneuver.

Once reached, the controller regulates the position to maintain the desired distance.

Finally, Figure 17 shows the consumed energy during the simulation (magenta), as well as the energy recovered by regenerative braking (green).

These results can be seen in video 1.

2) SUDDEN BRAKING OF THE PRECEDING VEHICLE

The second test is a test of avoiding collision in case of a sudden braking of the vehicle ahead. The goal of this test is to verify that the truck brakes preserving the safety distance in all cases. With this objective, the leader's speed profile is defined in Figure 18:

Figure 19 shows the speeds during the simulation. The truck speed is shown in blue, the truck desired speed in green and the speed of the leader's speed profile in yellow. The leader is running at 20m/s and when it reaches 35s, it suddenly brakes. At the beginning, the truck is running at 15 m/s. It must reach the preceding vehicle, so it accelerates until

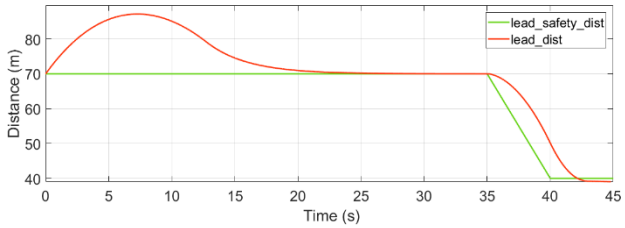

FIGURE 20. Distance between vehicles during the braking maneuver.

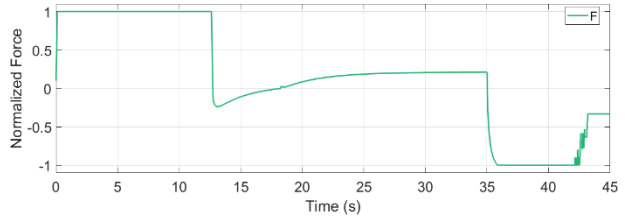

FIGURE 21. Accelerator / brake force during the maneuver.

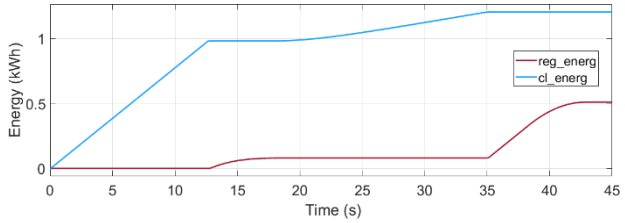

FIGURE 22. Consumed and regenerated energy during the braking maneuver.

it reaches the desired speed according with (76), and then it follows the desired speed profile until 20 m/s, keeping the safety distance (72) allowed by the preceding vehicle. When t=35 s, the preceding vehicle initiates the braking maneuver until stopping, i.e. the final speed is 0 m/s.

The distance between both vehicles is shown in Figure 20. At the beginning the vehicles are separated because the leader has a higher initial speed. Then the truck reaches the speed 20 m/s that allows to maintain the safety distance of 70 m, obtained from (72). Finally, the leader brakes suddenly and the trailer stops preserving the minimum safe distance of $d_0 = 40$ m.

As can be seen in Figure 19 and in Figure 20, in the first phase the truck accelerates to the maximum to reach the safety distance with the leader. Then the vehicle decelerates until it adapts its speed to the preceding vehicle one. Finally, the trailer brakes strongly to stop without reaching the leader.

Figure 21 includes the normalized driving force showing how the vehicle is accelerating or braking. This figure shows that, at the beginning, the vehicle accelerates with its maximum capacity until it reaches the safety distance with the preceding vehicle. After that, it adapts its driving force keeping the safety distance. When the preceding vehicle brakes, the truck brakes also with its maximum capacity until stopping.

Finally, the consumed energy (blue) and the energy recovered by the regenerative brake (magenta) are shown in Figure 22. In this case, the recovered energy is 40% of

the total. This is due to a heavy braking produced by the truck to avoid collision.

These results can be seen in video 2.

B. TRAJECTORY TRACKING

The simulation reproduces a trajectory tracking maneuver.

The trajectory is defined with the expression

$$y = x - 200 \cdot \sin(0.005 \cdot x)\, m \tag{77}$$

The leader will follow this trajectory and the truck must also follow it, being as close as possible to the leader, applying the adaptive cruise control. In this simulation d_p is calculated as:

$$d_p = 8.5 + (u_1 - 12) \cdot 0,1 \tag{78}$$

The vehicle is connected to the overhead line and the SOC constraint for the battery is not applied. Overtaking is not considered.

Figure 23 shows the leader and follower trajectories, being both trajectories very similar, as can be seen in the upper plot, with less than 0.05 m of lateral displacement between them, as can be seen in the lower plot.

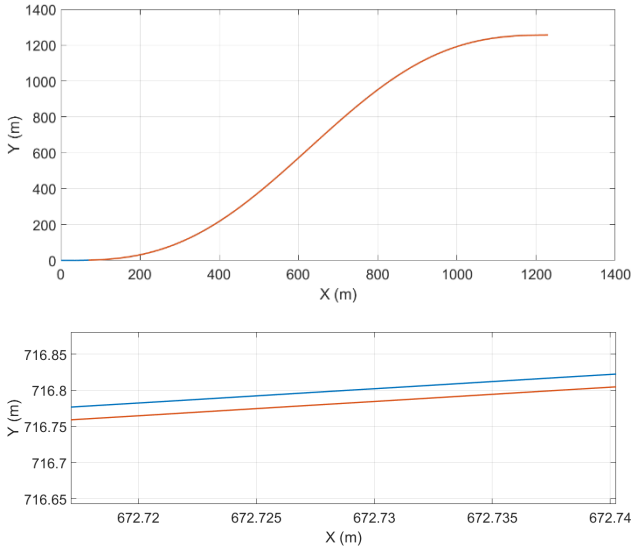

FIGURE 23. Trajectories in the trajectory tracking maneuver.

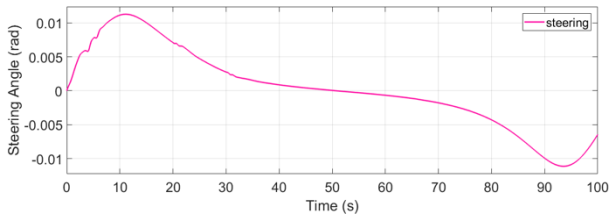

FIGURE 24. Steering angle in the trajectory tracking maneuver.

Figure 24 presents the truck steering angle, in rad.

Figure 25 shows the yaw angle for both vehicles. The truck (blue tractor and purple semitrailer) yaw angle is the same as for the leader (green), but with a small delay in time because the follower reaches later the same portion of the road.

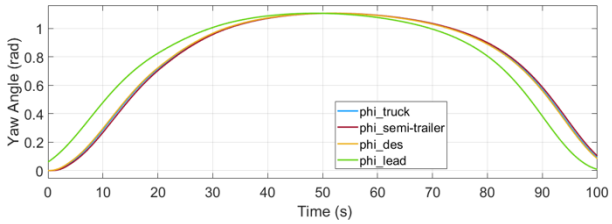

FIGURE 25. Yaw angles in the trajectory tracking maneuver.

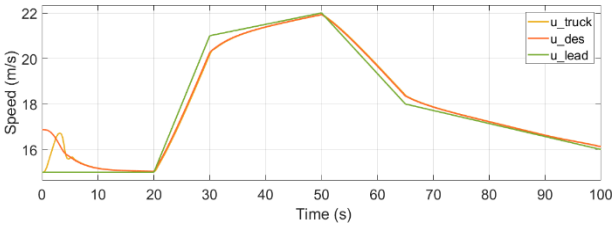

FIGURE 26. Velocities in the trajectory tracking maneuver.

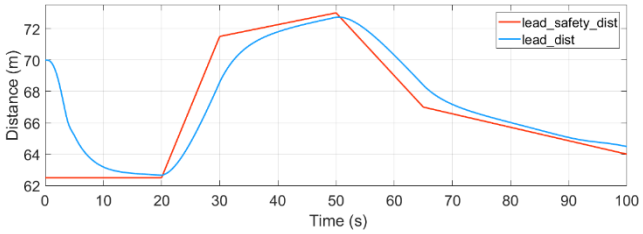

FIGURE 27. Safety distance in the trajectory tracking maneuver.

The trailer must keep a safe distance because the adaptive cruise control is active. Figure 26 represents the longitudinal velocity for the leader (green), the desired truck velocity (red) and the real truck speed (yellow).

With these velocities, the distance between vehicles (in blue) is close to the calculated safety distance (in red), as is shown in Figure 27.

These results can be seen in video 3.

C. OVERTAKING MANEUVER

The overtaking maneuver obeys the following rules:

- The truck must maintain the safety distance with the preceding vehicle at least 15 s and the constraint (55) is active. If the preceding vehicle accelerates and the distance is higher than the safety distance, this time resets to 0.
- The preceding vehicle speed must be lower than 23 m/s. The maximum truck speed is 25 m/s, imposed by constraint (50).
- If the preceding vehicle accelerates during the overtaking, the truck must abort the maneuver and return to its lane.
- The truck will not overtake if it has not enough battery, because it is disconnected from the overhead contact line when leaves its lane.
- If there is other vehicle in the left lane, the safety constraint (57) is activated preserving a safe distance between them.

- The truck will return to its lane when the distance with the overtaken vehicle is greater than a preestablished value.

When the truck initiates the overtaking, the constraint (55) is deactivated and the constraint (57) is activated, and the controller switches to the left lane trajectory constraint for tracking it. And when the truck is finishing the overtaking, it switches again to the right lane trajectory constraint.

The simulation model is the full model including the batteries SOC model (discharging when disconnected and charging when connected).

This simulation reproduces an overtaking in a two lanes road, in which both lanes have the same direction, including a third vehicle in the left lane.

The paths for the left and right lanes are:

$$\begin{aligned} y_l &= x - 400 \cdot \sin(0.0025 \cdot x)\, m \\ y_r &= x - 400 \cdot \sin(0.0025 \cdot x) + 3.75\, m \end{aligned} \tag{79}$$

Figure 28 shows the leader's speed profile. The leader starts the simulation with a constant speed of 15 m/s. The vehicle in the left lane begins the simulation being in parallel with the truck in with a speed of 21.5 m/s. This speed will be reduced to 21 m/s at the end of the overtaking maneuver. These speed profiles are shown in Figure 28.

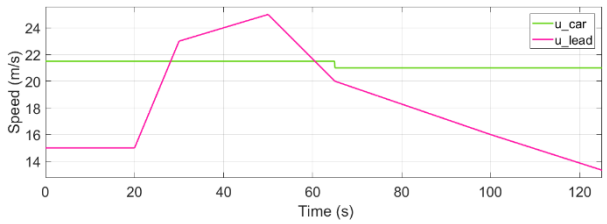

FIGURE 28. Speed profile for the leader and the vehicle in the left lane.

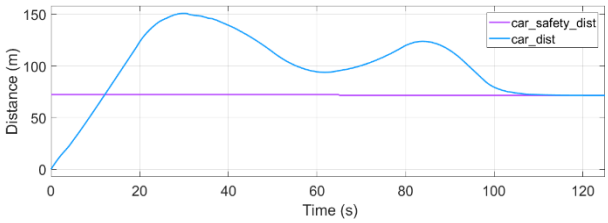

FIGURE 29. Distance between the truck and the vehicle in the left lane.

The leader speed is constant at the beginning, and when the truck is initiating the overtaking at t=20s, it accelerates. But, because of the leader velocity reaches more than 23 m/s, the truck must abort the overtaking keeping its lane. The overtaking will be initiated again when the conditions become favorable.

Figure 29 presents the distance between the truck and the vehicle in the left lane. This plot shows how this distance preserves the safety condition stablished in (55).

Figure 30 shows the different velocities involved the simulation: leader (magenta), vehicle in the left lane (green), desired truck speed (blue) and real truck speed (purple).

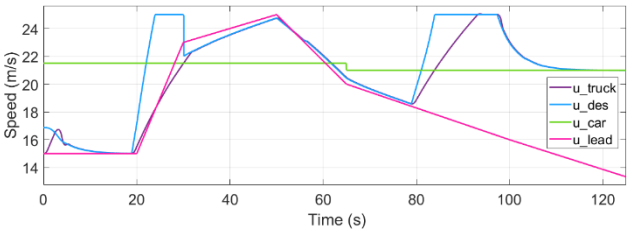

FIGURE 30. Velocities in the trajectory tracking maneuver.

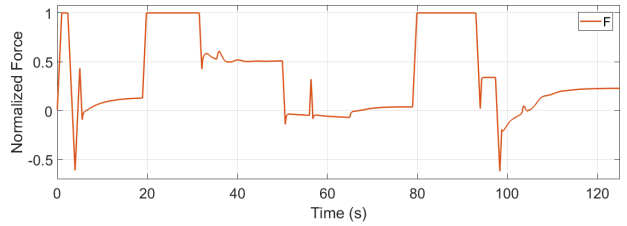

FIGURE 31. Driving/braking force.

Following the evolution of the different velocities, Figure 30 shows that, at the beginning, the truck approaches to the leader, and when it is at the safety distance, it keeps its velocity the same as the leader. After 15s, the desired truck speed changes to 25m/s starting the overtaking, that is allowed because the distance with the vehicle in the left lane is enough. But in this moment, the leader accelerates, and when it reaches 23 m/s, the truck aborts the overtaking, as seen in the plot between t=20s and t=30s.

The truck follows the leader until t=80s. Then the truck starts the overtaking again and, in this case, it completes the maneuver.

Figure 31 shows the results for the inputs. This plot includes the normalized input force, showing how, at the beginning and when the truck is initiating the overtaking, the truck applies maximum force. The plot also shows the braking actuation.

These results can be seen in video 4.

Figure 32 includes the different electrical variables involved in the simulation.

The upper plot shows the pantograph status: 1 means that it is connected to the overhead contact line (when the truck is in the right lane), and 0 means disconnected (when the truck is in the left lane).

The central plot includes the battery SOC. This plot shows how, when the pantograph is connected, the battery is charging and SOC increases, while when the pantograph is disconnected, the SOC decreases.

The lower plot shows the consumed and the recovered energy.

D. BATTERIES SIZING

The procedure to sizing the batteries is to consider the most unfavorable overtaking situation. The batteries size will be obtained by developing successive simulations until achieving the expected results. The parameter to be modified is the

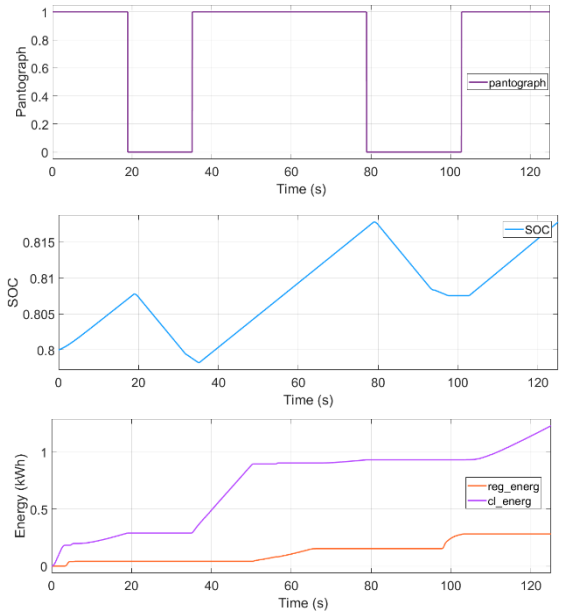

FIGURE 32. Electrical variables involved in the simulation.

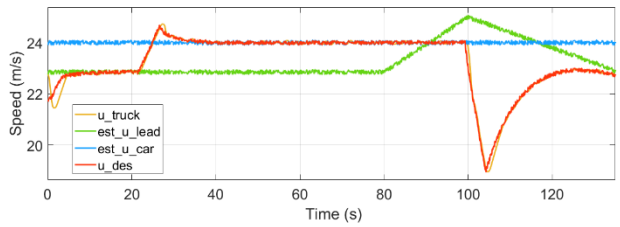

FIGURE 33. Speed of the different vehicles obtained by the simulated sensors during the simulation of battery dimensioning.

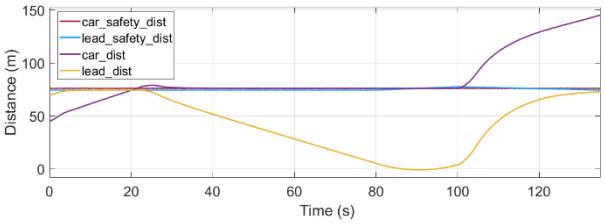

FIGURE 34. Distance between different vehicles during the simulation of battery dimensioning.

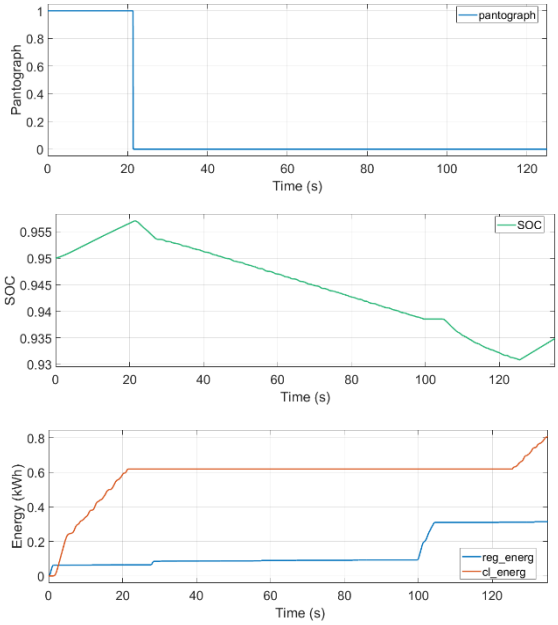

FIGURE 35. Value of the electrical variables during the simulation of battery dimensioning.

number of cells in parallel, since the number of cells in series is determined by the battery voltage. The simulation model is also the full model including the batteries SOC.

1) MOST UNFAVORABLE MANEUVER

The most unfavorable overtaking maneuver for the batteries is the maneuver in which the vehicle that is on the left lane is circulating at a constant speed of 24 m/s, limiting the overtaking speed of the truck. The leader is circulating at a speed of 23 m/s, which is the limit for the truck to decide overtaking. However, when the truck is almost finishing the overtaking, the leader accelerates to 25 m/s, higher than that of the car in the left lane. Therefore, the truck decides to abort the overtaking maneuver, decelerating slightly to reach the safety distance with the leader and returning to the right lane, connecting the pantograph to the overhead line.

The speeds of the three vehicles are shown in Figure 33, where the speed of the leader is in green, the car on the left in blue, the desired speed calculated by the truck in red and the front vehicle speed in yellow. The speeds shown are those collected by a simulated sensor, therefore some noise appears in the signals.

Figure 34 shows the gap with the vehicle in the left lane and the leader as well as the safety distance between both cars. The truck maintains the safety distance with the leader until overtaking. At that time, it keeps a safe distance from the car driving on the left. When the truck has slightly overtaken the leader, the latter accelerates so the truck decides to abort the maneuver returning to its lane. The maneuver needs 120 s.

Figure 35 shows the electrical variables during the simulation, in this case for a battery of 90 cells in parallel. It shows how the pantograph remains disconnected during the maneuver, obtaining the energy from the batteries. Finally, the consumed and regenerated energy during the simulation are also shown.

2) BATTERY DIMENSIONING

Next, the previous simulation is repeated for different battery configurations. The criterion for selecting a battery is to use 50% of its maximum energy. A larger number is not chosen because it is necessary to consider that factors such as temperature or temporary deterioration of the battery could reduce its performance, so it is necessary a wide margin that prevents the vehicle running out of power during the overtaking. The results are shown in Figure 36.

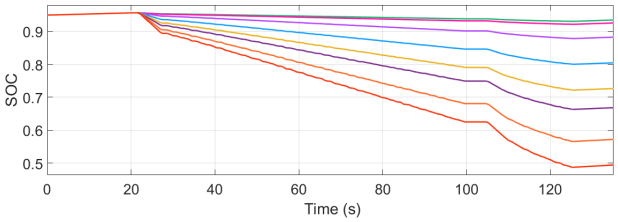

FIGURE 36. States of charge of the batteries with the different configurations.

TABLE 1. Comparison of different battery configurations.

Nº cells in series	Nº cells in parallel	Nº total cells	Battery energy (kwh)	Battery weight (kg)	Color in the plot
190	90	17100	139.20	736	
190	67	12730	103.62	548	
190	30	5700	46.40	245	
190	15	2850	23.20	123	
190	10	1900	15.47	82	
190	8	1520	12.37	65	
190	6	1140	9.28	49	
190	5	950	7.73	41	

The battery configurations are shown in Table 1:

As shown in Table 1, a 950-cell battery consumes just under 50% of the total battery charge so it meets the objective. This battery has a weight of 41 Kg.

V. CONCLUSIONS

In this paper, a simulation model has been developed, representing faithfully the expected behavior of an autonomous driving vehicle constituted by a trailer composition, working through a pantograph connection to an overhead line.

The autonomous driving control system is based on MPC and it has been designed for a truck with electric driving system powered by an overhead line, using a battery pack for maneuvers that require the disconnection of the pantograph, as is the case of overtaking.

In the first part of the paper, the articulated vehicle model has been presented. The model includes the mechanical behavior as well as the electrical behavior for the powertrain, including the batteries.

Next, a control system based on MPC has been implemented. The MPC has been especially useful for this application, stablishing limitations for guarantying the lateral and yaw trailer stability as well as for controlling the SOC for the batteries when the vehicle is disconnected from the overhead line.

Once the controller has been implemented, different simulations have been developed in which the trailer carried out different maneuvers autonomously. These maneuvers are adaptive cruise control, trajectory tracking, and overtaking in safety conditions, aborting the maneuver if conditions compromise the safety. The adaptive cruise and the trajectory tracking simulations have been used to adjust the controller's parameters. The overtaking simulation has been used as a general test in a complex maneuver including the basic maneuvers and the battery management when overtaking.

TABLE 2. Parameters values.

Parameter	Description	Value
M_1	Tractor mass	7500 Kg
J_1	Tractor inertia	2.66e+04 Kgm^2
M_2	Semi-trailer mass	32550 Kg
J_2	Semi-trailer inertia	5.35e+05 Kg·m^2
a	Dist tractor front - c.o.g.	1.11 m
b	Dist. tractor rear axle - c.o.g.	2.49 m
c	Gage / 2	1.10 m
d	Dist. semitrailer axle - c.o.g.	3.15 m
e	Dist. kingpin semitrailer - c.o.g.	4.98 m
f	Dist. kingpin tractor dist. - c.o.g.	1.81 m
Cy_f	Front tires cornering stiffness	1.84e+05 N/rad
Cy_r	Rear tires cornering stiffness	8.11e+04 N/rad
Cy_s	Semitrailer tires cornering stiffness	1.12e+06 N/rad
P	Power	476 HP
R	Wheel radius	0.35 m
V	Overhead line Voltage	700 V

TABLE 3. Battery model parameters.

Par.	a0	a1	a2	a3	a4	a5	a6
V_{oc}	3	13,43	-90,04	284,3	-453,6	355,9	-108,9
$R_{int}(D)$	0,048	0,144	-0,458	0,497	-0,129	-0,05	0
$R_s(D)$	0,146	-1,059	4,87	-10,13	9,508	-3,302	0
$C_s(D)$	0,742	9,068	-30,71	32,55	-7,36	-3,462	0
$R_m(D)$	1,742	-33,84	228,9	-712,8	1118,	-859,2	-0,12
$C_m(D)$	239,5	-14.76	264.2	-825.0	947.2	-371.2	0
$R_{int}(C)$	0,051	0,208	-1,115	2,166	-1,777	0,53	0
$R_s(C)$	0,113	0,972	5,093	-11,28	10,91	-3,85	0
$C_s(C)$	0,994	14,52	-91,98	199	-179,7	-57,92	0
$R_m(C)$	1,656	-35,02	246,6	-78.56	1251	-971,9	292,7
$C_m(C)$	216,5	28.31	-166.4	431.2	-491.5	199.6	0
R_h	0,148	-1,198	3,595	-4,36	1,834	0	0
C_h	493.9	3.0e7	-1.0e8	2.0e8	-9.0e7	0	0

The simulation results have been satisfactory obtaining a maximum lateral displacement error of 0.1 m in the trajectory tracking and a safe SOC higher than 70% with the control policy followed in the overtaking maneuver, demonstrating the feasibility of the proposed control.

Finally, the model has been also used for determining the minimum size of the batteries. With this optimization, the size of the batteries has been significantly reduced with respect to the batteries used in a pure electrical truck that does not use the overhead contact line as primary energy source.

The behavior presented by the model during the simulations is similar to the expected, performing all maneuvers autonomously in conditions of stability and safety. However, this paper only includes simulation results. The validations including the comparative results between the model and the real vehicle will be object of future research, building, for example, a scaled prototype or introducing sensors in a real vehicle and making itineraries in a test circuit that will be simulated later with the model, comparing both.

APPENDIX A
VEHICLE PARAMETERS

See Table 2.

APPENDIX B
BATTERY MODEL PARAMETERS

See Table 3.

REFERENCES

[1] Siemens. [Online]. Available: https://www.siemens.com/global/en/home/products/mobility/road-solutions/electromobility/ehighway.html
[2] Siemens. [Online]. Available: https://cleantechnica.com/2017/11/12/siemens-ehighway-heavy-duty-trucks-continue-california/
[3] J. M. Anderson, K. Nidhi, K. D. Stanley, P. Sorensen, C. Samaras, and T. A. Oluwatola, *Autonomous Vehicle Technology: A Guide for Policymakers*. Santa Monica, CA, USA: RAND Corp., 2016. [Online]. Available: https://www.rand.org/pubs/research_reports/RR443-2.html, doi: 10.7249/RR443-2.
[4] T. Litman. (2017). Autonomous Vehicle Implementation Predictions. Victoria Transport Policy Institute. [Online]. Available: https://www.vtpi.org/avip.pdf
[5] S. J. Qin and T. A. Badgwell, "A survey of industrial model predictive control technology," *Control Eng. Pract.*, vol. 11, no. 7, pp. 733–764, 2003, doi: 10.1016/S0967-0661(02)00186-7.
[6] G. Mantovani and L. Ferrarini, "Temperature control of a commercial building with model predictive control techniques," *IEEE Trans. Ind. Electron.*, vol. 62, no. 4, pp. 2651–2660, Apr. 2015, doi: 10.1109/TIE.2014.2387095.
[7] J.-Q. Wang, S. E. Li, Y. Zheng, and X.-Y. Lu, "Longitudinal collision mitigation via coordinated braking of multiple vehicles using model predictive control," *Integr. Comput.-Aided Eng.*, vol. 22, no. 2, pp. 171–185, 2015, doi: 10.3233/ICA-150486.
[8] S. Di Cairano, H. E. Tseng, D. Bernardini, and A. Bemporad, "Vehicle yaw stability control by coordinated active front steering and differential braking in the tire sideslip angles domain," *IEEE Trans. Control Syst. Technol.*, vol. 21, no. 4, pp. 1236–1248, Jul. 2013, doi: 10.1109/TCST.2012.2198886.
[9] B. Zhu, H. Tazvinga, and X. Xia, "Switched model predictive control for energy dispatching of a photovoltaic-diesel-battery hybrid power system," *IEEE Trans. Control Syst. Technol.*, vol. 23, no. 3, pp. 1229–1236, May 2015, doi: 10.1109/TCST.2014.2361800.
[10] D. Hrovat, S. Di Cairano, H. E. Tseng, and I. V. Kolmanovsky, "The development of model predictive control in automotive industry: A survey," in *Proc. IEEE Int. Conf. Control Appl. (CCA)*, Oct. 2012, pp. 295–302, doi: 10.1109/CCA.2012.6402735.
[11] C. E. Garcia, D. M. Prett, and M. Morari, "Model predictive control: Theory and practice—A survey," *Automatica*, vol. 25, no. 3, pp. 335–348, 1989, doi: 10.1016/0005-1098(89)90002-2.
[12] F. Borrelli, P. Falcone, T. Keviczky, J. Asgari, and D. Hrovat, "MPC-based approach to active steering for autonomous vehicle systems," *Int. J. Veh. Auto. Syst.*, vol. 3, nos. 2–4, pp. 265–291, 2005, doi: 10.1504/IJVAS.2005.008237.
[13] P. Falcone, H. E. Tseng, J. Asgari, F. Borrelli, and D. Hrovat, "Integrated braking and steering model predictive control approach in autonomous vehicles," *IFAC Proc. Volumes*, vol. 40 no. 10, pp. 273–278, 2007, doi: 10.3182/20070820-3-US-2918.00038.
[14] S. Lefèvre, A. Carvalho, and F. Borrelli, "Autonomous car following: A learning-based approach," in *Proc. IEEE Intell. Vehicles Symp. (IV)*, Jun./Jul. 2015, pp. 920–926, doi: 10.1109/IVS.2015.7225802.
[15] V. Turri, Y. Kim, J. Guanetti, K. H. Johansson, and F. Borrelli, "A model predictive controller for non-cooperative eco-platooning," in *Proc. IEEE Amer. Control Conf. (ACC)*, May 2017, pp. 2309–2314, doi: 10.23919/ACC.2017.7963297.
[16] Y. Zheng, S. E. Li, K. Li, F. Borrelli, and J. K. Hedrick, "Distributed model predictive control for heterogeneous vehicle platoons under unidirectional topologies," *IEEE Trans. Control Syst. Technol*, vol. 25, no. 3, pp. 899–910, May 2017, doi: 10.1109/TCST.2016.2594588.
[17] J. Zhou and H. Peng, "Range policy of adaptive cruise control vehicles for improved flow stability and string stability," *IEEE Trans. Intell. Transp. Syst.*, vol. 6, no. 2, pp. 229–237, Jun. 2005, doi: 10.1109/TITS.2005.848359.
[18] J. Guanetti, Y. Kim, and F. Borrelli, "Control of connected and automated vehicles: State of the art and future challenges," *Annu. Rev. Control*, vol. 45, pp. 18–40, Apr. 2018, doi: 10.1016/j.arcontrol.2018.04.011.
[19] J. Zhang, F.-Y. Wang, K. Wang, W.-H. Lin, X. Xu, and C. Chen, "Data-driven intelligent transportation systems: A survey," *IEEE Trans. Intell. Transp. Syst.*, vol. 12, no. 4, pp. 1624–1639, Dec. 2011, doi: 10.1109/TITS.2011.2158001.
[20] J. Felez, G. Romero, J. Maroto, and M. L. Martinez, "Simulation of multibody systems using multi-bond graphs," in *Bond Graph Modelling of Engineering Systems*. New York, NY, USA: Springer, 2011, pp. 323–354, doi: 10.1007/978-1-4419-9368-7_9.
[21] J. Felez, "A method for minimizing the set of equations in bond graph systems with causal loops," in *Bond Graphs for Modelling, Control and Fault Diagnosis of Engineering Systems*. Cham, Switzerland: Springer, 2017, pp. 27–46, doi: 10.1007/978-3-319-47434-2_2.
[22] J. Maroto, E. Delso, J. Felez, and J. M. Cabanellas, "Real-time traffic simulation with a microscopic model," *IEEE Trans. Intell. Transp. Syst.*, vol. 7, no. 4, pp. 513–527, Dec. 2006, doi: 10.1109/TITS.2006.883937.
[23] Y. Cao, R. C. Kroeze, and P. T. Krein, "Multi-timescale parametric electrical battery model for use in dynamic electric vehicle simulations," *IEEE Trans. Transport. Electrific.*, vol. 2, no. 4, pp. 432–442, Dec. 2016, doi: 10.1109/TTE.2016.2569069.
[24] M. Chen and G. A. Rincon-Mora, "Accurate electrical battery model capable of predicting runtime and I-V performance," *IEEE Trans. Energy Convers.*, vol. 21, no. 2, pp. 504–511, Jun. 2006, doi: 10.1109/TEC.2006.874229.
[25] M. F. J. Luijten, "Lateral dynamic behaviour of articulated commercial vehicles," M.S. thesis, Eindhoven Univ. Technol., Eindhoven, The Netherlands, 2010. [Online]. Available: http://www.mate.tue.nl/mate/pdfs/12050.pdf
[26] T. Stanger and L. del Re, "A model predictive cooperative adaptive cruise control approach," in *Proc. IEEE Amer. Control Conf. (ACC)*, Jun. 2013, pp. 1374–1379, doi: 10.1109/ACC.2013.6580028.
[27] Volvo. [Online]. Available: https://www.aggman.com/volvo-introduces-volvo-enhanced-cruise-adaptive-cruise-control-with-proactive-braking/

JESUS FELEZ (M'97–SM'18) received the Mechanical Engineer and Ph.D. degrees from the University of Zaragoza, Spain, in 1985 and 1989, respectively.

He became a Full Professor at the Universidad Politecnica de Madrid (UPM), Spain, in 1997. He has served as the Thesis Advisor for 30 master's theses and eight Ph.D. dissertations. He has published over 70 technical papers and has been actively involved in over 30 R&D national and international projects with public competitive funding, and over 50 relevant R&D projects with private companies.

His research interests are in the area of technologies applied to the future railways, in particular to train control systems. He is the expert in the field of railway technology, a member of the scientific commission for the railway sector in Spain, and the Head of the Research Group in Simulation in mechanical engineering at UPM.

CARLOS GARCÍA-SANCHEZ received the Industrial Engineer degree (major in mechanical engineering) from the Universidad Politécnica de Madrid in 2017, where he is currently pursuing the M.Sc. degree in industrial engineering, and the double Diploma degree with the Politecnico di Milano. His research interests are mainly focused on mechanical design, simulation, and vehicles technologies.

JOSÉ ANTONIO LOZANO was a Researcher at the Railway Technology Research Group from 2009 to 2013. He is currently an Associate Professor in the field of mechanical engineering with the Department of Mechanical Engineering, Chemistry, and Industrial Design, Universidad Politecnica de Madrid (UPM). He is currently a member of the Research Group in Simulation in mechanical engineering at UPM. He has over 35 papers in international publications and over 20 contributions in international conferences. His main R&D lines are in simulation, bond graphs, railway traction, noise and vibration, automobiles, traffic accident reconstruction, and machines design.